Spin-crossover Transition Coupled with Another Solid–Solid Phase Transition for Iron(II) Thiocyanate Complexes Chelated with Alkylated *N*-(Di-2-pyridylmethylene)anilines

Yuya Oso, Daisuke Kanatsuki, Shuichi Saito, Takashi Nogami, and Takayuki Ishida*
Department of Applied Physics and Chemistry, The University of Electro-Communications, Chofu, Tokyo 182-8585

(Received April 14, 2008; CL-080384; E-mail: ishi@pc.uec.ac.jp)

We have prepared spin-crossover [$FeL_2(NCS)_2$] complexes chelated with alkylated *N*-(di-2-pyridylmethylene)anilines. The wider irreversible thermal loop across room temperature was observed with the longer alkyl chain introduced (ΔT_C = ca. 90 K for a *n*-$C_{16}H_{33}$ derivative). Pressurization prohibits the solid–solid phase transition, leading to the reversible spin crossover.

Spin-crossover (SCO) phenomenon is a reversible low-spin/high-spin transition by external stimuli such as heat.[1] We can often find SCO in iron(II) compounds having an FeN_6 octahedron.[2] Bistability near room temperature due to a wide thermal hysteresis is a key to future applications to memories and displays.[3] Multifunctional materials are of increasing interest.[4] We have investigated SCO systems where long alkyl chains are introduced to improve intermolecular interaction.[5] We will report here SCO phenomena on [$Fe^{II}L_2(NCS)_2$] (L = alkylated *N*-(di-2-pyridylmethylene)anilines) and a very wide thermal loop across room temperature. There have been many reports on liquid-crystalline SCO materials,[4,6] but the phase diagram of the present compounds is unique.

Ligands were easily prepared from condensation of di-2-pyridyl ketone with *p*-alkylanilines.[7] Complexation with iron(II) thiocyanate was conducted in 1-propanol under nitrogen. The products (see Figure 1 for the molecular structures) were characterized by means of elemental analysis and spectroscopic methods.[8] The specimens did not involve any crystal solvent.

The crystal structures of **1** at 100 and 400 K were successfully determined (Figure 1),[9] thanks to the SCO phase transition taking place in a single-crystal-to-single-crystal manner. Two SCN groups occupy a cis position. One pyridine N atom does not participate in ligation. The Fe–N bonds fell in the typical range of the low- and high-spin FeN_6 octahedra.[10] The Fe–N bonds are elongated by 10% on the average on heating to 400 K. Unfortunately, no single crystal of **2** suitable for crystallographic analysis could be obtained, but we assumed that **2** underwent a similar SCO phase transition.

The magnetic measurements of powder specimens of them on a SQUID magnetometer revealed that this family exhibited SCO behavior. Compound **2** and related alkyl homologues showed a large thermal cycle (Figure 2a); namely, in the first heating process the $\chi_{mol}T$ value of **2** increased around $T_{C\uparrow}$ = 300 K[11] ($S = 0 \rightarrow S = 2$). When the specimen was then cooled, the $\chi_{mol}T$ value did not trace the previous one. Instead, the $\chi_{mol}T$ value decreased around $T_{C\downarrow}$ = 210 K ($S = 2 \rightarrow S = 0$). Similarly, a derivative having R = *n*-$C_{14}H_{29}$ showed SCO phenomena at $T_{C\uparrow}$ = 290 K and $T_{C\downarrow}$ = 250 K. From a closer look at the initial heating curve of **2**, we found a sharp jump at 375 K. The C_{14} derivative exhibited a jump at 380 K in the initial heating measurement. On the other hand, no hysteresis was observed for **1** ($T_{C\uparrow\downarrow}$ = 270 K) and derivatives with shorter alkyl groups such as R = *n*-C_4H_9 ($T_{C\uparrow\downarrow}$ = 320 K). We observed the wider loop, when the longer alkyl group was introduced.

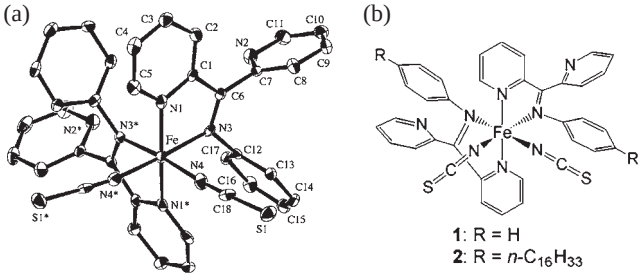

Figure 1. (a) ORTEP drawing of **1** with thermal ellipsoids at the 50% probability level at 100 K. Hydrogen atoms are omitted. Symmetry operation code for * is $1 - x, y, 1/2 - z$. (b) Structural formula. Selected bond lengths are as follows: Fe–N1, 1.999(3) [2.185(7)]; Fe–N3, 1.966(2) [2.233(7)]; Fe–N4, 1.954(3) [2.091(5)] Å. Bond lengths measured at 400 K are shown in square brackets.

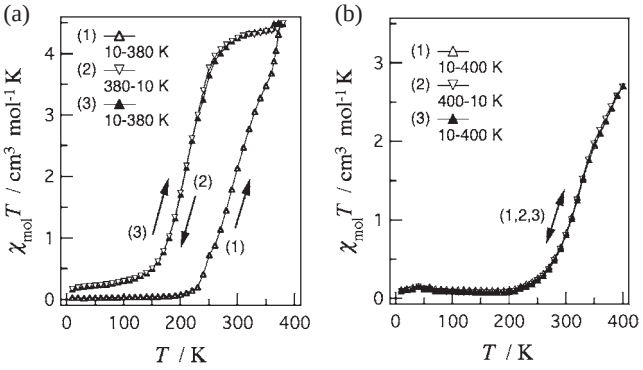

Figure 2. The $\chi_{mol}T$ vs. T plots for **2** under ambient pressure (a) and under an applied pressure of 0.11 GPa (b). Temperature scan sequences are denoted with arrows. A static filed of 5000 Oe was applied.

We found that these loops did not originate in intrinsic SCO hysteresis, because the $\chi_{mol}T$ curve in the second heating process never traced the initial heating one. Actually, completely reversible SCO was recorded when the magnetic measurements were performed under the limited thermal conditions below the temperature where the jump occurred.

To clarify the origin of this irreversibility, we simultaneously measured XRD–DSC of **2**. A phase transition was characterized at 375 K, as indicated by endo- and exothermal peaks in DSC measurements (Figure 3a). The XRD profile was drastically changed across 375 K. We also found another peak at 390 K and attributed it to a melting point. An additional peak around 400 K became ambiguous at a slow heating rate or after a long interval (the inset). The XRD profile remained almost the same

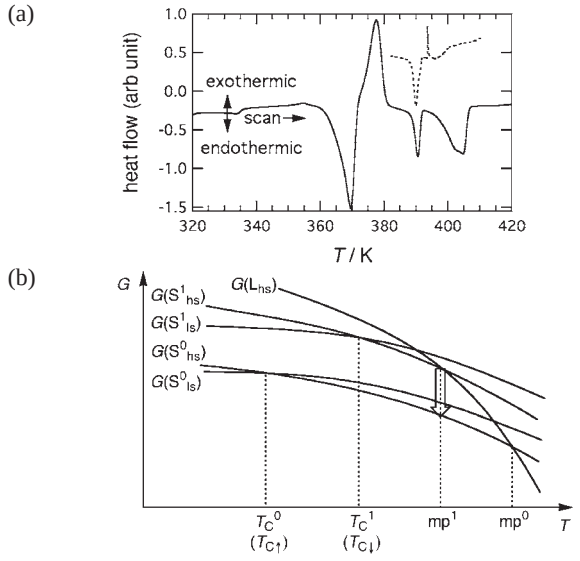

Figure 3. (a) DSC measurements on **2** at a warming rate of $3\,\mathrm{K\,min^{-1}}$. A dotted line in the inset shows the data when the temperature scan was suspended at 393 K for 180 min. (b) Free energy diagram for **2**.

across 390 K, but it gradually melted as indicated by the disappearance of the XRD peaks. An overheated portion might remain above the melting point.

A relaxation from a meta-stable phase to a ground phase is suggested by the exothermic peak at 375 K (ca. 25 kJ/mol). Each phase has low-spin (ls) and high-spin (hs) states. A G vs. T diagram is usually convenient (Figure 3b), where we named the phases as S^1 (meta-stable solid), S^0 (stable solid), and L (liquid). L_{ls} is energetically unstable and undetectable. The thermal cycle of **2** is interpreted as: ${S^1}_{ls} \rightarrow (T_C{}^1) \rightarrow {S^1}_{hs} \rightarrow (mp^1) \rightarrow {S^0}_{hs} \rightarrow (mp^0) \rightarrow L_{hs}$ on heating and $L_{hs} \rightarrow (mp^0) \rightarrow {S^0}_{hs} \rightarrow (T_C{}^0) \rightarrow {S^0}_{ls}$ on cooling. Since mp^1 is located lower than mp^0, a partial melt induces an exothermic solid–solid phase transition or resolidifying occurs immediately after the melt (an arrow in Figure 3b).

Two phenomena were separated by applying pressure, demonstrating that the magnetic properties shown in Figure 2a are caused by the combination of the SCO and solid–solid phase transitions. We measured the SCO of **2** using a Cu–Be clamp-type cylinder cell (ElectroLAB, Japan).[12] As Figure 2b shows, the melt phase transition was removed, but the SCO transition remained at 330 K, that is, shifted higher by 30 K, under 0.11 GPa. The thermal loop completely disappeared in a temperature range available. A pressure effect on the SCO transition temperature was confirmed on a similar experiment on **1**; the T_C was elevated only by ca. 40 K under 0.23 GPa.

Pressure effects to stabilize low-temperature phases are common, and the transition temperatures are elevated according to the Clapayron–Clausius equation. In the present case, the melt largely depends on the volume change due to the bulky substituents, and consequently the mp is more sensitive to pressure than the SCO T_C. On applying pressure on **2**, $T_C{}^1$ is left behind below 400 K while the mp^1 is shifted over 400 K.

A problem still remains; we could not obtain S^0 of **2** by recrystallization from any alcoholic solvents investigated here. It may be because the solvation sphere around each molecule of **2** favors molecular packing suitable for the meta-stable phase.

In summary, the thermal cycle of **2** showed a very wide irreversible loop. It behaves as a SCO compound with $T_C{}^1 = 300\,\mathrm{K}$, but once heated above 375 K it irreversibly became a SCO compound with $T_C{}^0 = 210\,\mathrm{K}$. Pressurization elevates the melting point and prohibits it to enter a stable phase. This work suggests a potential utility of **2** as a magnetic-detection pressure sensor as well as a write-once information storage material at ambient pressure.[13]

This work was supported by Grants-in-Aid for Scientific Research (Nos. 17550166 and 19550135) from the Ministry of Education, Culture, Sports, Science and Technology, Japan.

References and Notes

1 P. Gütlich, H. A. Goodwin, *Spin Crossover in Transition Metal Compounds I, II, and III*, Springer-Verlag, Berlin, **2004**; P. Gütlich, A. Hauser, H. Spiering, *Angew. Chem., Int. Ed. Engl.* **1994**, *33*, 2024.

2 J. A. Real, A. B. Gaspar, M. C. Muñoz, *Dalton Trans.* **2005**, 2062; J. A. Real, A. B. Gaspar, V. Niel, M. C. Muñoz, *Coord. Chem. Rev.* **2003**, *236*, 121.

3 J.-F. Létard, P. Guionneau, E. Codjovi, O. Lavastre, G. Bravic, D. Chasseau, O. Kahn, *J. Am. Chem. Soc.* **1997**, *119*, 10861; S. Hayami, Z. Gu, H. Yoshiki, A. Fujishima, O. Sato, *J. Am. Chem. Soc.* **2001**, *123*, 11644; S. Cobo, G. Molnár, J. A. Real, A. Bousseksou, *Angew. Chem., Int. Ed.* **2006**, *45*, 5786; E. Coronado, J. R. Galán-Mascarós, M. Monrabal-Capilla, J. García-Marthinez, P. Pardo-Ibánez, *Adv. Mater.* **2007**, *19*, 1359.

4 A. B. Gaspar, V. Ksenofontov, M. Seredyuk, P. Gütlich, *Coord. Chem. Rev.* **2005**, *249*, 2661.

5 H. Inokuchi, G. Saito, P. Wu, K. Seki, T. B. Tang, T. Mori, K. Imaeda, T. Enoki, Y. Higuchi, K. Inaka, N. Yasuoka, *Chem. Lett.* **1986**, 1263.

6 W. Zhang, F. Zhao, T. Liu, M. Yuan, Z.-M. Wang, S. Gao, *Inorg. Chem.* **2007**, *46*, 2541; S. Hayami, K. Danjobara, K. Inoue, Y. Ogawa, N. Matsumoto, Y. Maeda, *Adv. Mater.* **2004**, *16*, 869; M. Seredyuk, A. B. Gaspar, V. Ksenofontov, S. Reiman, Y. Galyametdinov, W. Haase, E. Entschler, P. Gütlich, *Chem. Mater.* **2006**, *18*, 2513; O. Roubeau, J. M. A. Gomez, E. Balskus, J. J. A. Kolnaar, J. G. Haasnoot, J. Reedijk, *New J. Chem.* **2001**, *25*, 144; S. Hayami, R. Moriyama, Y. Shigeyoshi, R. Kawajiri, T. Mitani, M. Akita, K. Inoue, Y. Maeda, *Inorg. Chem.* **2005**, *44*, 7295.

7 J. Suh, D. W. Min, *J. Org. Chem.* **1991**, *56*, 5710.

8 **1**: mp >250 °C. Anal. Calcd for $C_{36}H_{26}FeN_8S_2$: C, 62.61; H, 3.79; N, 16.23; S, 9.29%. Found: C, 62.47; H, 3.73; N, 15.63; S, 8.84%. **2**: mp 117–134 °C. Anal. Calcd for $C_{68}H_{90}FeN_8S_2$: C, 71.68; H, 7.96; N, 9.83; S, 5.63%. Found: C, 71.84; H, 8.16; N, 9.99; S, 5.34%.

9 Selected crystallographic data of **1**. At 100 K: monoclinic, $C2/c$, $a = 13.681(3)$, $b = 11.360(3)$, $c = 21.345(5)$Å, $\beta = 93.5819(17)^\circ$, $V = 3310.9(14)$ Å^3. At 400 K: monoclinic, $C2/c$, $a = 13.62(4)$, $b = 11.644(18)$, $c = 22.25(3)$ Å, $\beta = 92.617(10)^\circ$, $V = 3525(13)$ Å^3. For details, see CCDC 684391 and 684392.

10 B. Gallois, J.-A. Real, C. Hauw, J. Zarembowitch, *Inorg. Chem.* **1990**, *29*, 1152.

11 The T_C is defined by the temperature where $\mathrm{d}(\chi_{mol}T)/\mathrm{d}T$ is maximum, because a conventional $T_{1/2}$ value cannot be defined owing to a $\chi_{mol}T$ jump. An error within ±5 K was estimated.

12 Y. Uwatoko, *Koatsuryoku no Kagaku to Gijutsu* **2001**, *11*, 181; K. Yuza, T. Ishida, T. Nogami, *Chem. Lett.* **2005**, *34*, 974.

13 For experimental details, the $\chi_{mol}T$ vs. T plots on **1** and the C_4 and C_{14} derivatives, the results on **1** under pressure, the XRD profiles on **2** at 360 and 380 K, and the DSC profile on the C_{14} derivative, see Supporting Information, being available electronically on the CSJ-Journal Web site, http://www.csj.jp/jounals/chem-lett/index.html.

Published on the web (Advance View) June 14, 2008; doi:10.1246/cl.2008.760